Finite Element Analysis to determine the impact of Infill density on Mechanical Properties of 3D Printed Materials

Z Andleeb[1], H Khawaja[2]*, K Andersen[2], M Moatamedi[3]

1. Abyss Solutions, Islamabad, Pakistan
2. UiT-The Arctic University of Norway, Tromsø, Norway
3. Al Ghurair University, Dubai, United Arab Emirates

ABSTRACT

Additive manufacturing (AM) is the process in which objects are created through the layer-by-layer deposition of material that is controlled by a computer. The infill is the internal structure of the 3D printed model. It determines the strength, weight, cost, time, and overall quality of the part. Ranging from simple lines to more complex geometric shapes, infill patterns can affect a part's performance. This study aims to conduct a Numerical Analysis for cross pattern infills with various infill densities of 0%, 10%, 19, 28%, 64%, and 100%. CAD models were developed, and FEA Analysis was performed to compare the deformation and Von Mises stresses produced by a cuboid structure under 1 MPa compressional load. Linear Isotropic Material with Young's Modulus of 70 GPA and the Poisson ratio of 0.3 was used, and quarter symmetry was applied to reduce the mesh size. The results revealed that the increasing infill percentage decreases the deformation and Von Mises stresses produced in a body under compression loading. This study helps to determine optimal infill density for maximizing strength and minimizing the weight of the 3D printed part.

1. INTRODUCTION

1.1 Additive Manufacturing – Continuous Fiber Fabrication (CFF)

The Additive Manufacturing process completely deviates from the conventional manufacturing methods by producing parts in layers using chopped or continuous carbon fibers. The Continuous Fiber Fabrication (CFF) 3D printing is two steps per layer process [1]. First, a thermoplastic is extruded to form the infill and shells of the part; this serves as the matrix of the composite. Next, the continuous fiber is ironed into that matrix, fusing with the thermoplastic by use of a compatible resin coating, as shown in Figure 1. This process repeats layer by layer, forming the fibers into the backbone of the 3D printed part, while the thermoplastic acts as a skin [2].

*Corresponding Author: hassan.a.khawaja@uit.no

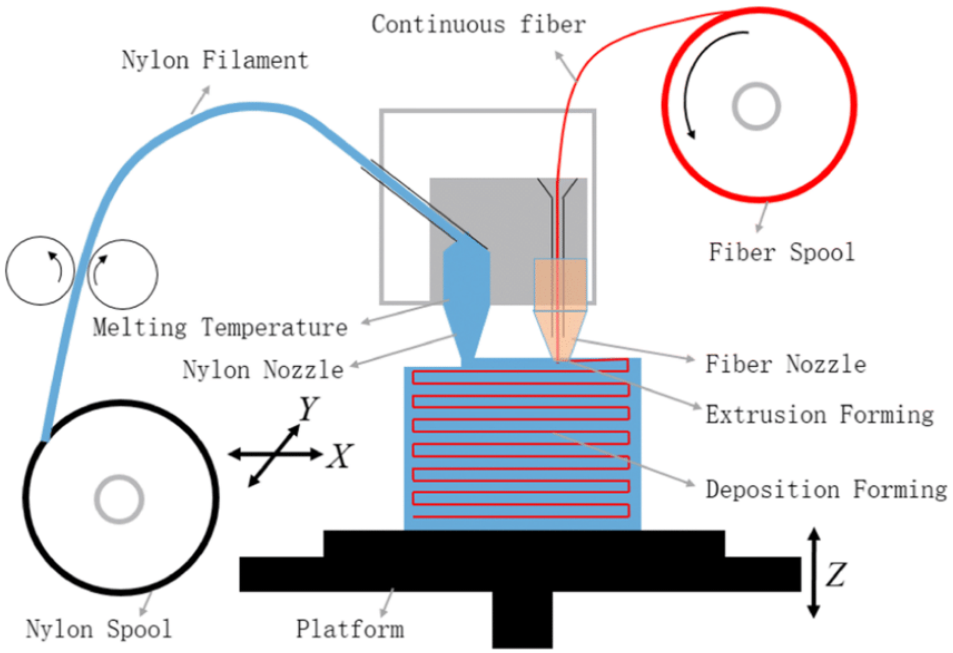

Figure 1: Schematic view of the 3D printing of Composite reinforced with continuous carbon fiber [3]

1.2 Finite Element Analysis

Finite Element Analysis (FEA) simulates the physical phenomena using numerical mathematical techniques by discretizing them into small elements [4-9]. The FEM material models are based on Continuum Mechanics; therefore, displacement and stress fields are assumed to be continuous within each discrete element [10-13]. The common problem with Continuous Fiber Fabrication (CFF) 3D printing method is the interfacial gaps between layers that do not conform with conventional continuum-based Finite Element Method (FEM) material models. Infill patterns that are a common weight reduction feature of 3D printing further adds complexity to numerical Modeling of 3D printed parts [14].

1.3 Infill patterns in 3D printing

Infill pattern is the material's structure and shape inside a 3D printed part. The ratio of plastic to space is defined as a print's infill density, close to 0% means the part is mostly hollow, while close to 100% means it is mostly solid [15,16]. Ranging from simple lines to more complex geometric shapes, infill patterns can affect a part's strength, weight, print time, and even flexibility, as shown in Figure 2. Across different slicer programs, there are many different infill patterns.

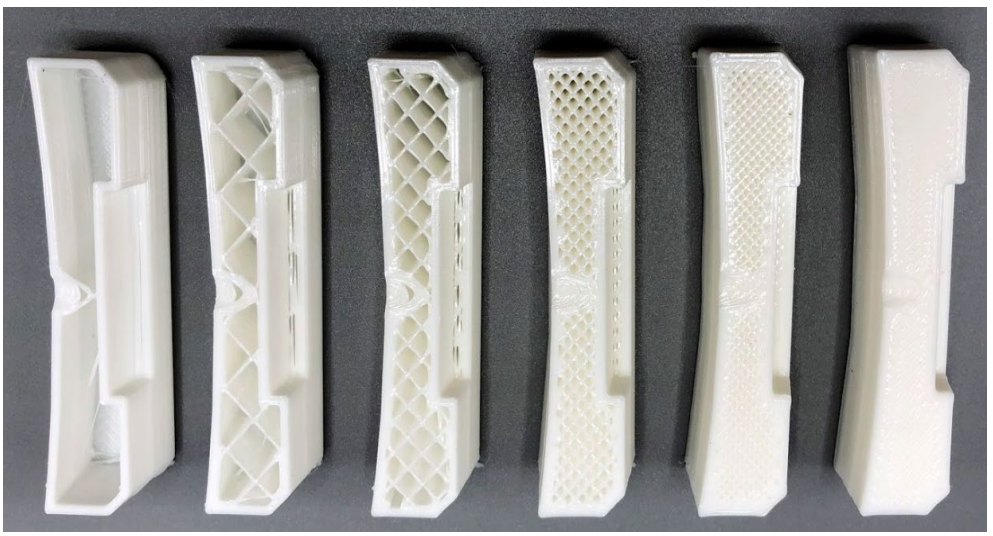

Figure 2: Cross-section of 3D printed parts with different infills [17]

2. METHODOLOGY

In this study, CAD Models were developed for five configurations, representing the percentage of infill density as calculated by Equation (1),

$$Infill\ (\%) = \frac{V - V_{hollow}}{V_{solid} - V_{hollow}} \tag{1}$$

where V is the volume of cuboid (mm^3), V_{hollow} is the volume of hollow cuboid (mm^3), and V_{solid} is the volume of solid cuboid (mm^3).

The infill densities under investigation were 0%, 10%, 19%, 28%, 64%, and 100% for deformation and Von-Mises stresses [8,18] under compressional load.

2.1. FEA (ANSYS® Explicit Dynamic)

The numerical analyses were performed in ANSYS® Workbench Explicit Dynamics [19]–[21] module to simulate the infill ratio under the same compressional load. The material assigned was Linear Isotropic Material with Young's Modulus of 70 GPA and Poisson ratio is 0.3. Quarter symmetry was applied to reduce mesh size, and mesh sensitivity analysis was performed to optimize the mesh. Quarter symmetry was applied to reduce mesh size. Dimension of the cuboid under investigation was 10 mm x 10 mm x 20 mm. Table 1 below shows five configurations based on different infill percentages chosen for this study. The problem is setup by applying quarter symmetry reducing mesh size as shown in Figure 3. Boundary conditions of compressive load of 1 MPa is applied to the top surface and fixed support in the bottom surface of as shown in Figure 4 and Figure 5. CAD Model and FEA Mesh are also illustrated for the various configurations in Figures 3-8. Mesh sensitivity analysis was performed to ensure the correctness of results.

Table 1: Volume of various Infills (%)

Configuration	Volume (mm^3)	$Infill\ (\%) = \frac{V - V_{hollow}}{V_{solid} - V_{hollow}}$
0	192.824 (hollow)	0 %
1	369.45	10 %
2	538.02	19 %
3	693.79	28 %
4	1348.4	64 %
5	2000 (solid)	100 %

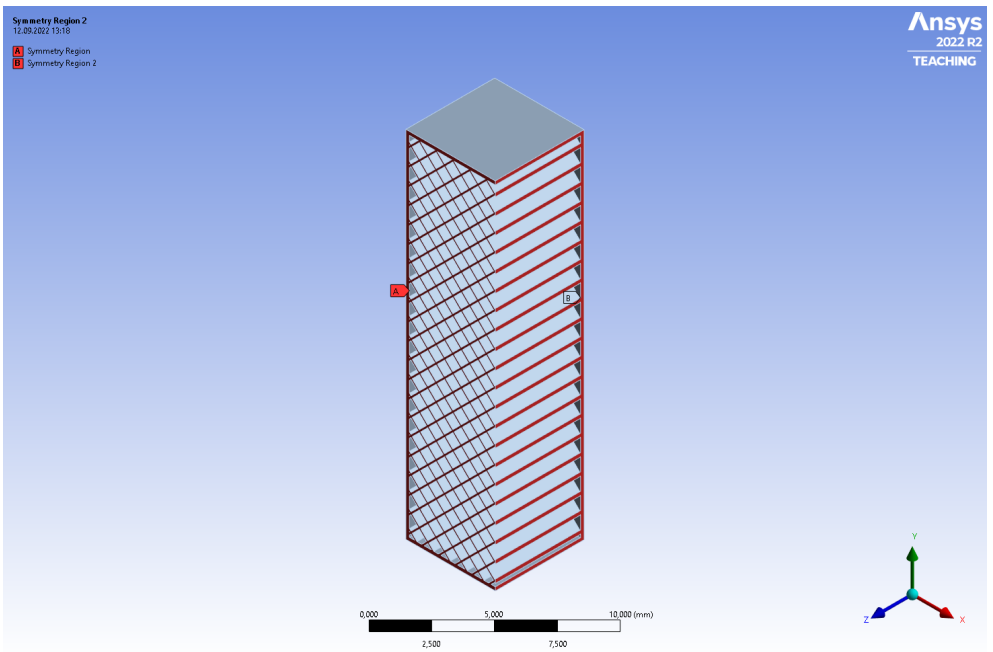

Figure 3: Quarter symmetry for mesh size reduction

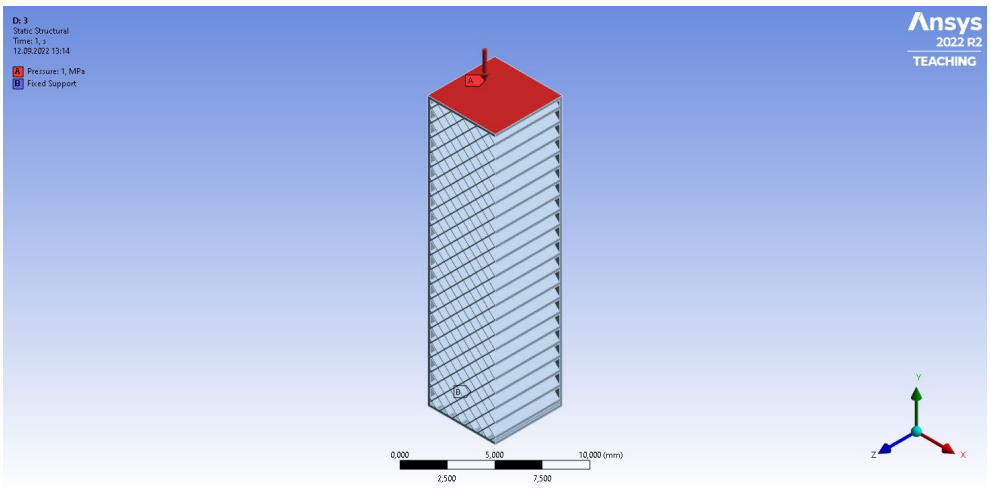

Figure 4: Boundary condition of compressive load of 1 MPa on the top surface

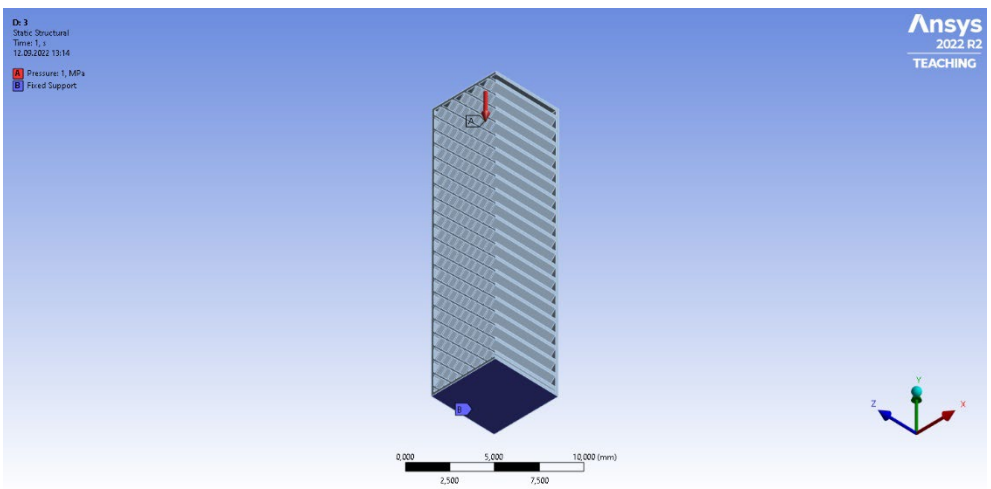

Figure 5: Fixed support in the bottom surface

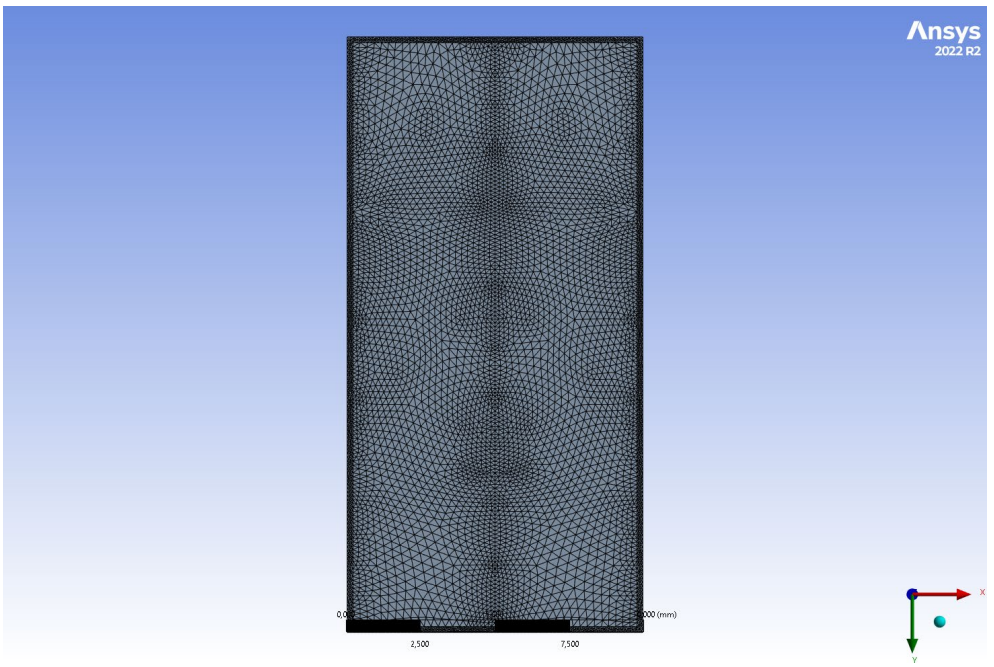

Figure 6: CAD Model and FEA Mesh of Configuration 0 (volume: 192.824 mm3), infill ratio of 0%

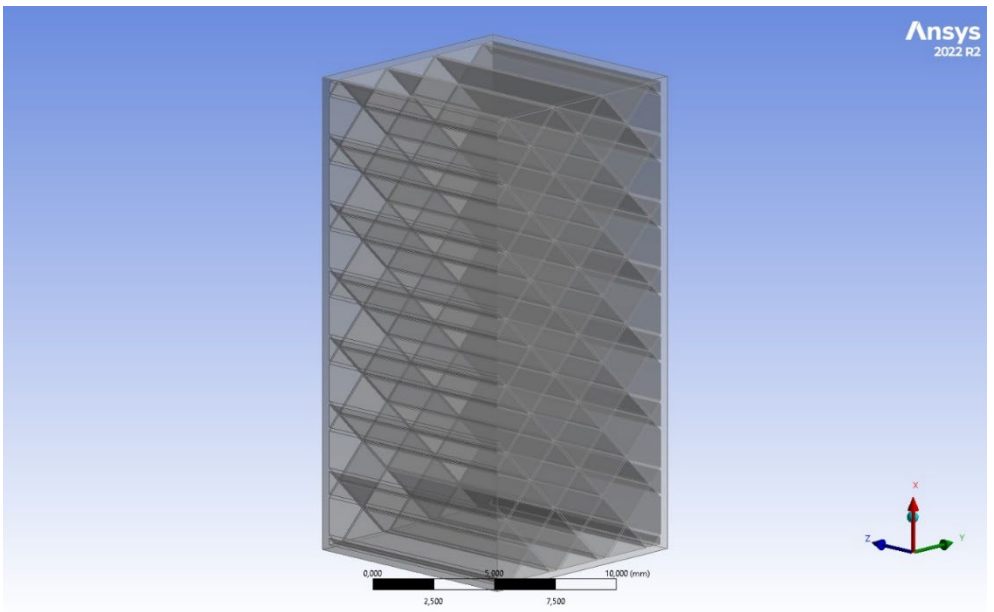

(a)

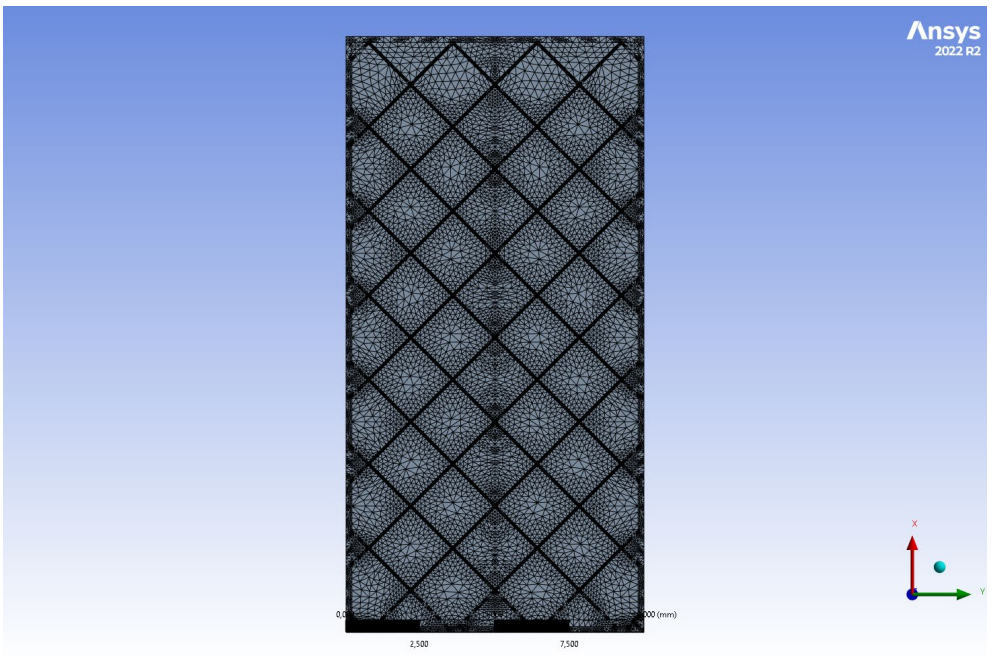

(b)

Figure 7: CAD Model and FEA Mesh of Configuration 1 (volume: 369.45 mm^3), infill ratio of 10%

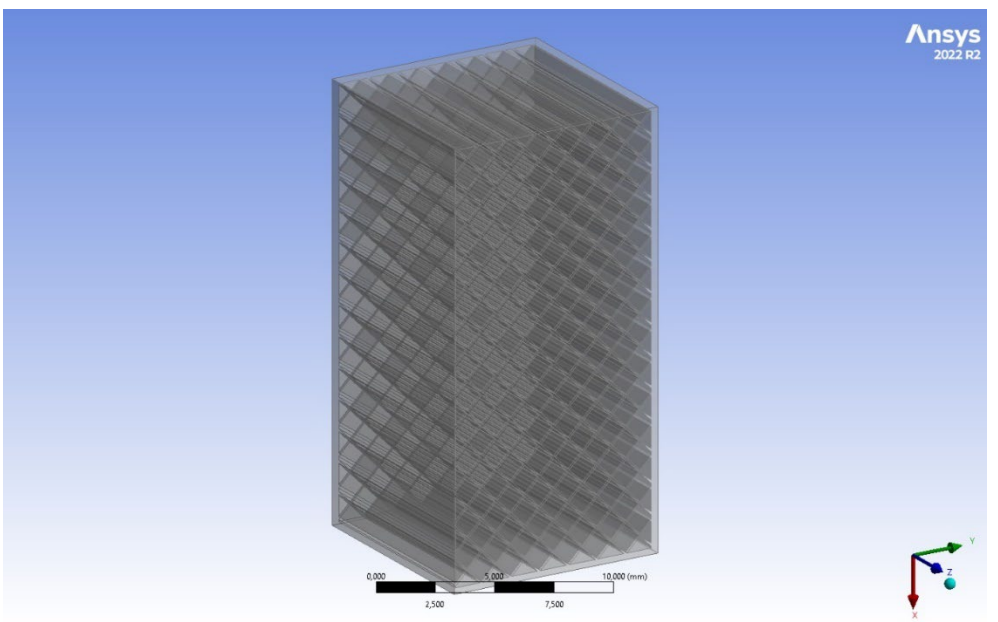

(a)

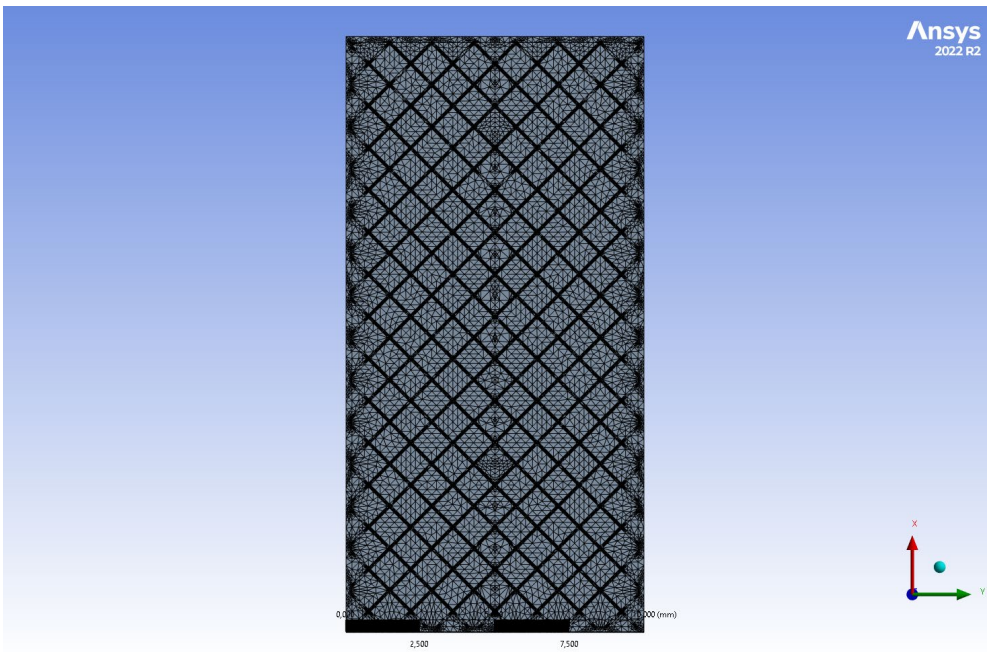

(b)

Figure 8: CAD Model and FEA Mesh of Configuration 2 (volume: 538.02 mm^3), infill ratio of 19%

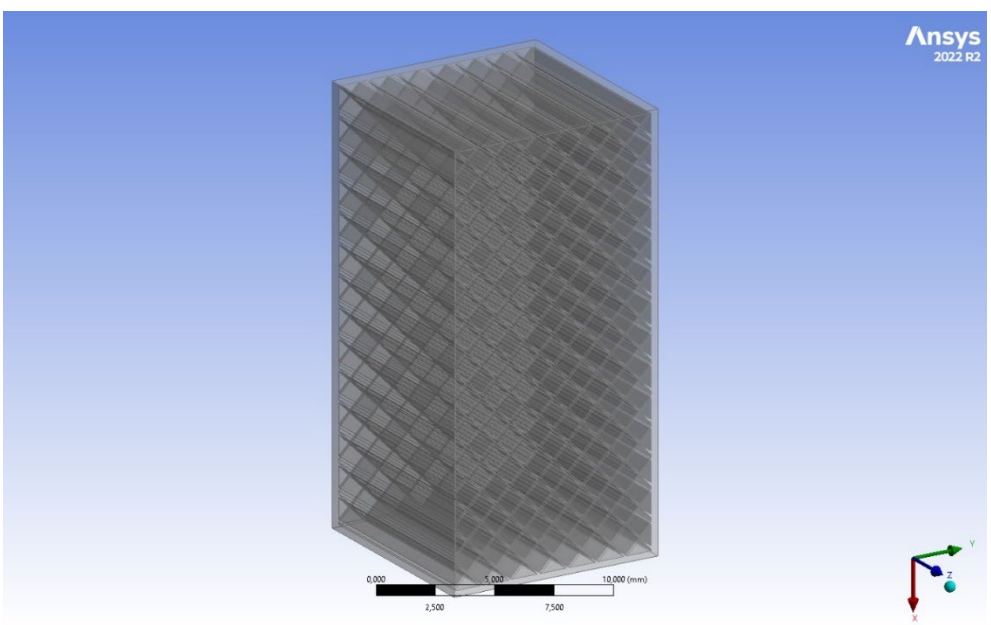

(a)

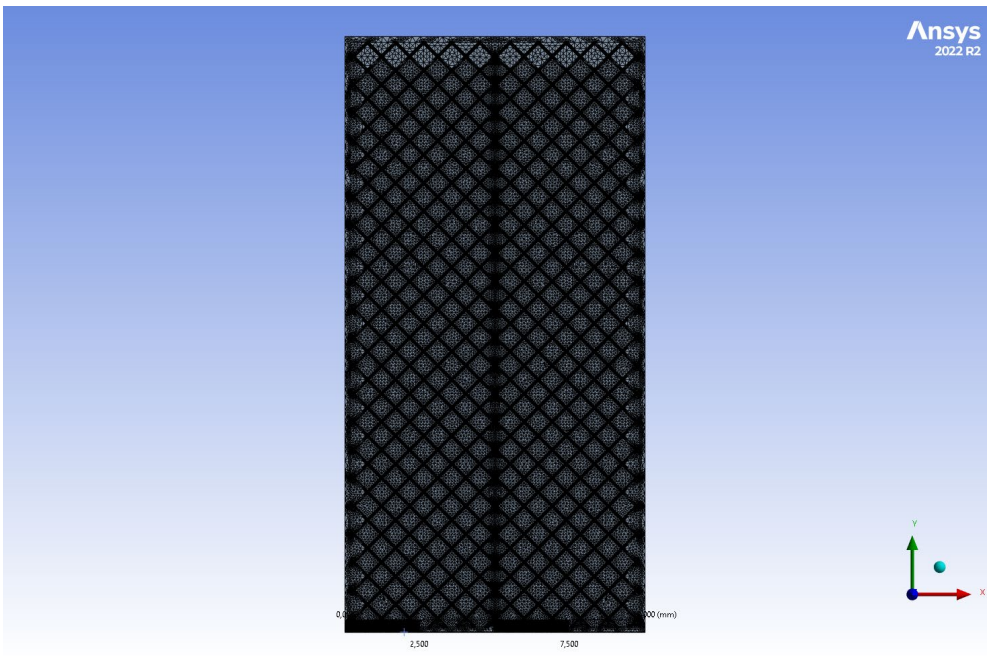

(b)

Figure 9: CAD Model and FEA Mesh of Configuration 3 (volume: 693.79 mm^3), infill ratio of 28%

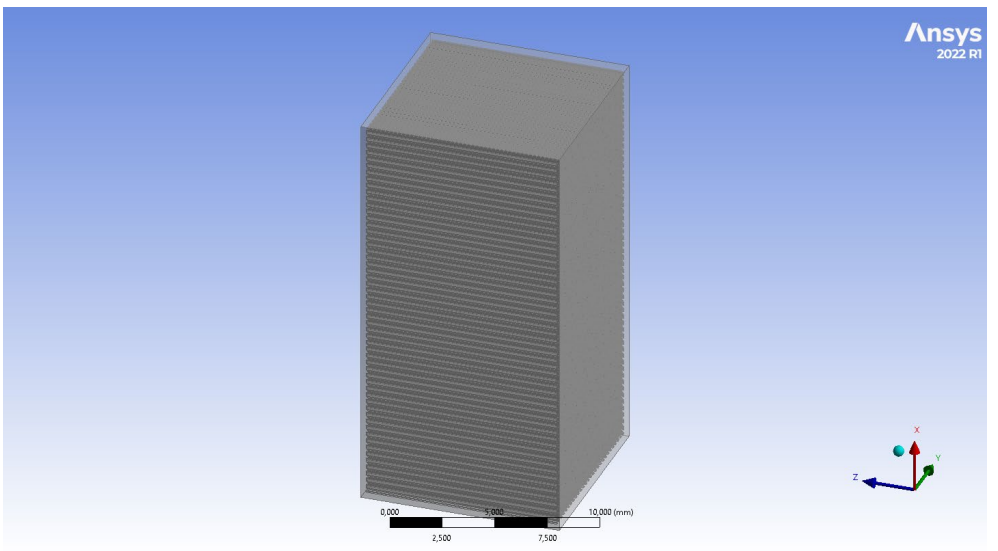

(a)

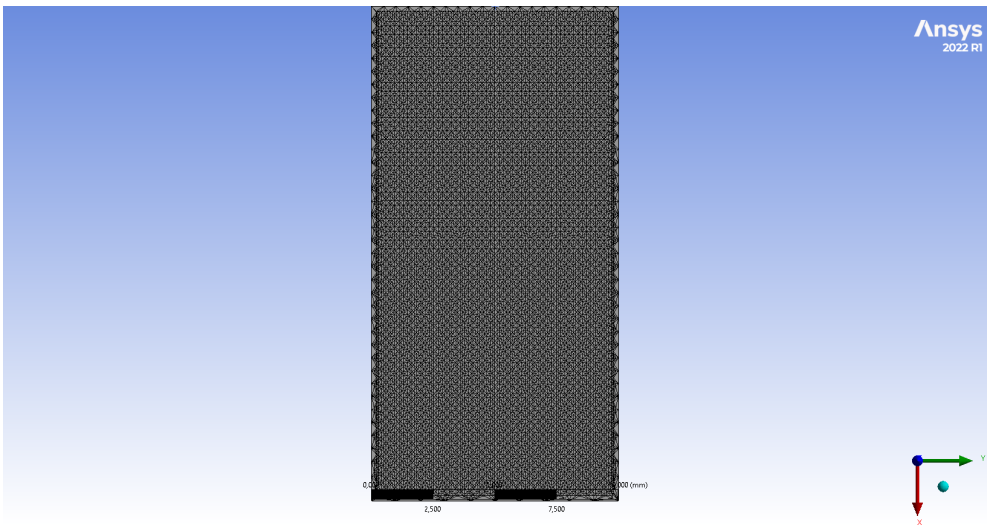

(b)

Figure 10: CAD Model and FEA Mesh of Configuration 4 (volume: 1348.4 mm^3), infill ratio of 64%

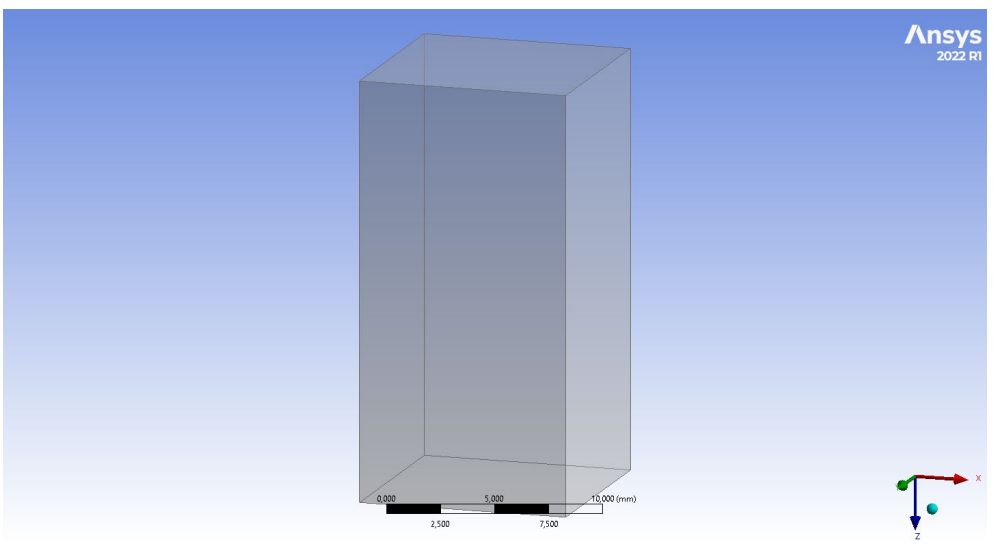

(a)

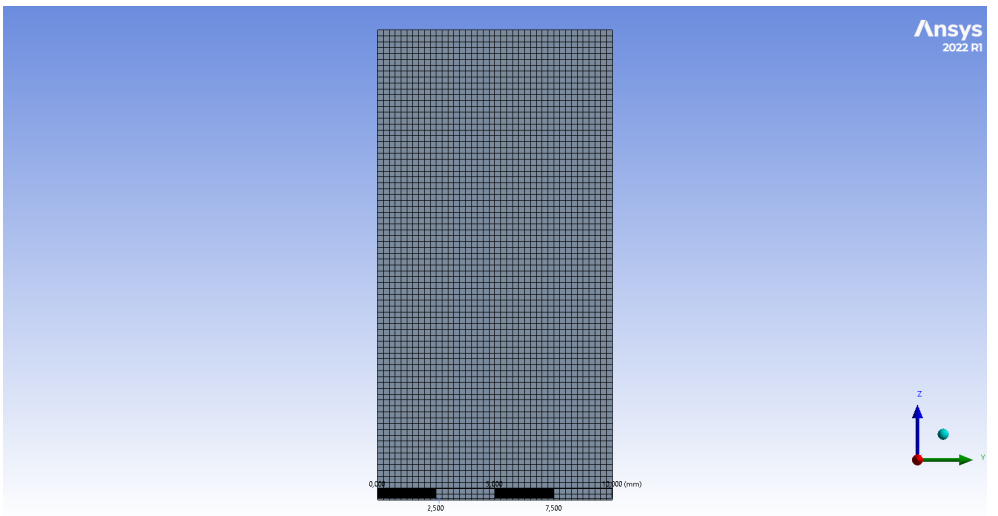

(b)

Figure 1: CAD Model and FEA Mesh of Configuration 5 (volume: 2000 mm^3), infill ratio of 100%

4 RESULTS AND DISCUSSION

The results reveal that the increasing infill percentage decreases the deformation and Von Mises stresses produced in a structure under compression loading. The Results are shown in Table 2.

Table 2: Deformation and Von-Mises Stress of various Infills (%)

Configuration	Volume (mm^3)	Infill ratio	Max. Deformation (mm)	Max. VM Stress (MPa)
0	192.824	0 %	0.36815	432.95
1	369.45	10 %	0.010921	79.051
2	538.02	19 %	0.0047711	24.534
3	693.79	28 %	0.0038717	24.227
4	1348.4	64 %	0.00091986	5.1365
5	2000	100 %	0.0002831	3.1881

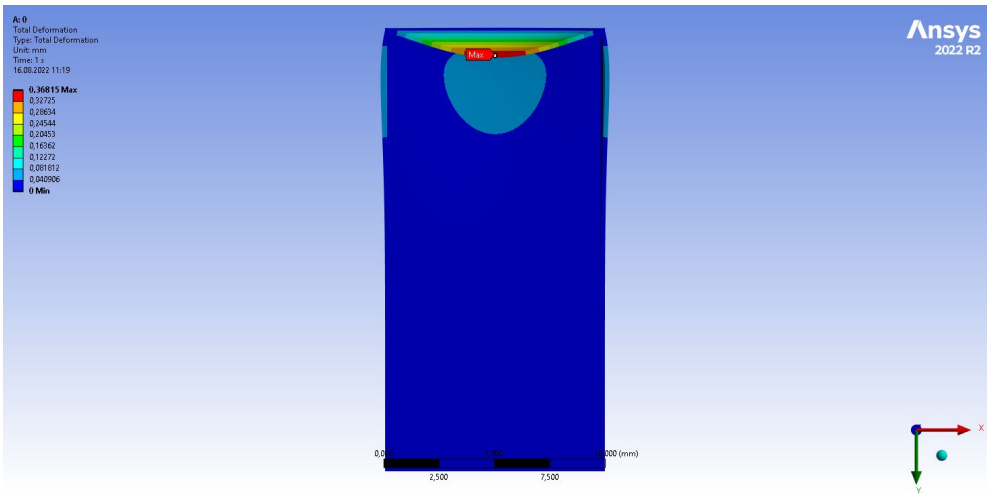

(a)

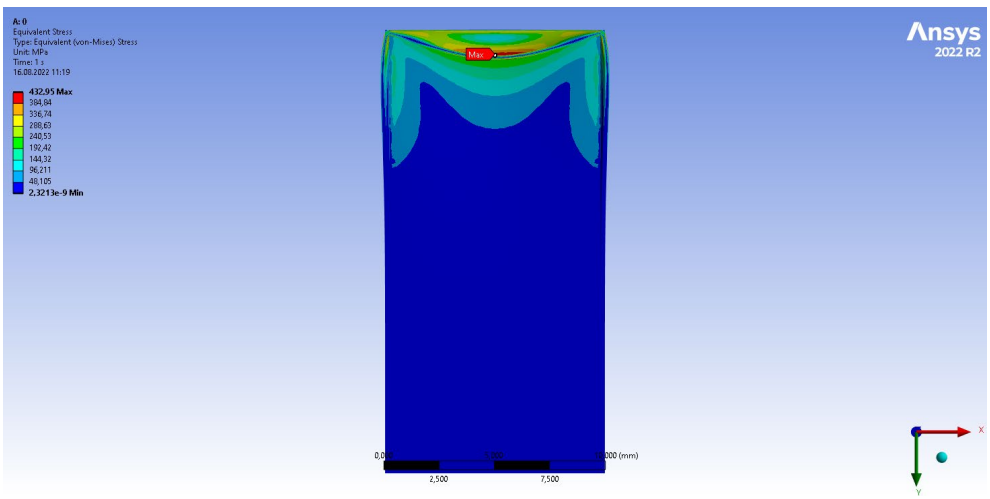

(b)

Figure 12: Max. Deformation (mm) and Von-Mises stress (MPa) of Configuration 0 (volume: 192.824 mm^3), infill ratio of 0%

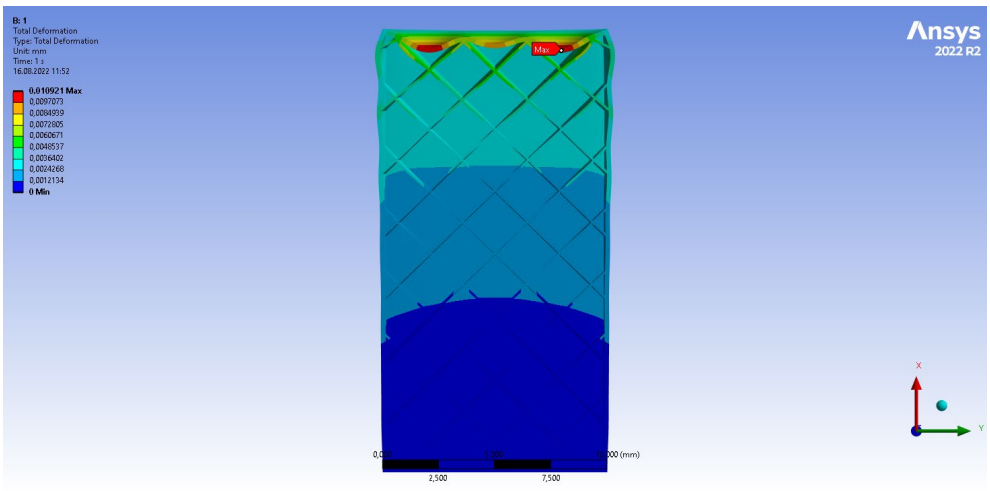

(a)

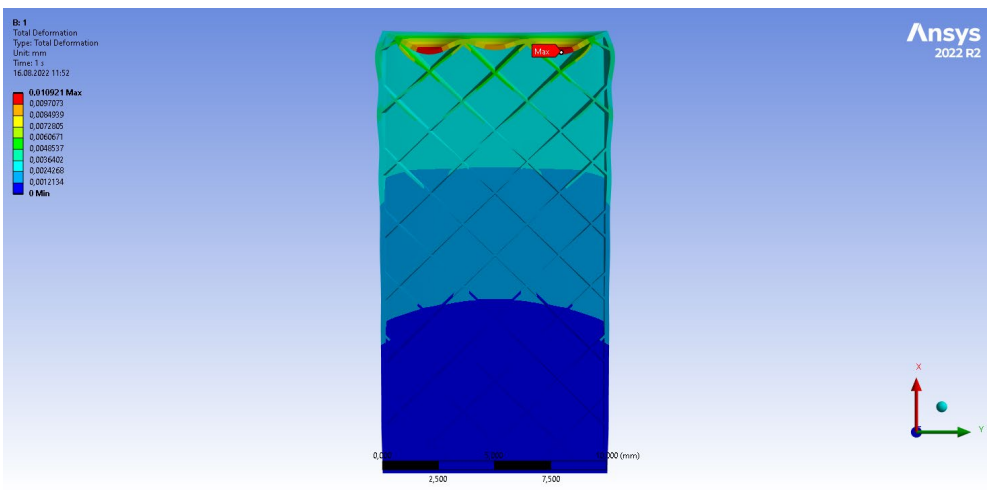

(b)

Figure 13: Max. Deformation (mm) and Von-Mises stress (MPa) of Configuration 1 (volume: 369.45 mm^3), infill ratio of 10%

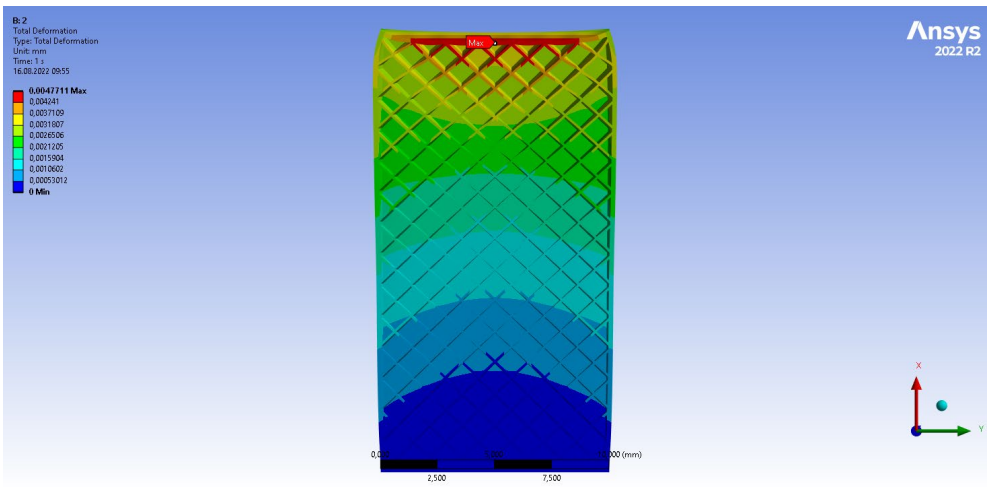

(a)

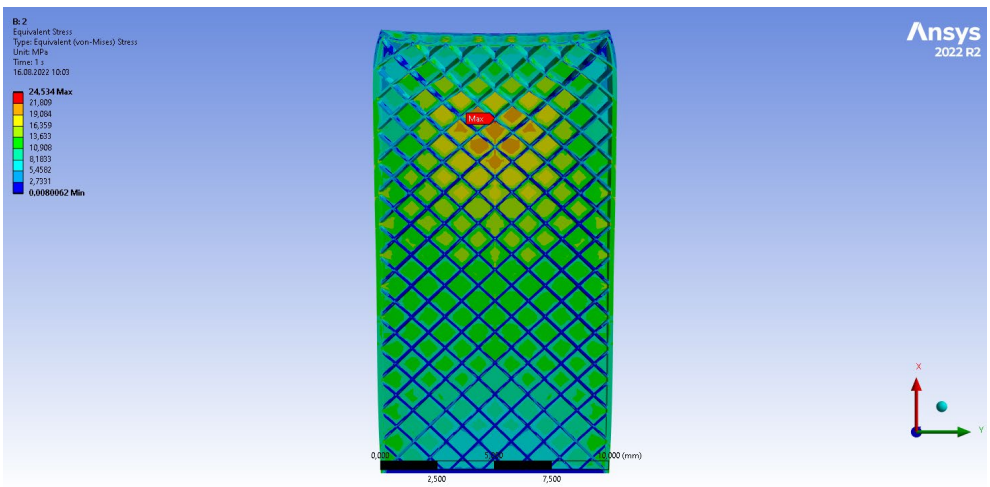

(b)

Figure 14: Max. Deformation (mm) and Von-Mises stress (MPa) of Configuration 2 (volume: 538.02 mm^3), infill ratio of 19%

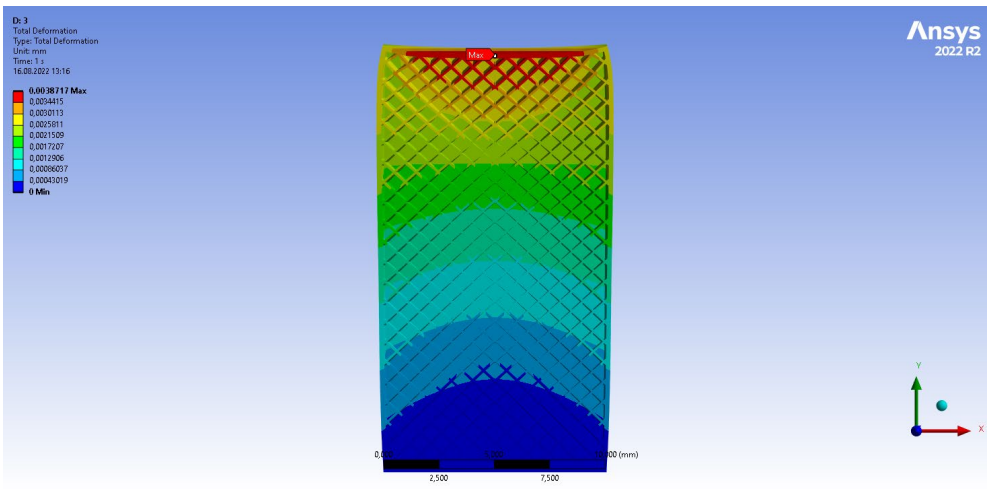

(a)

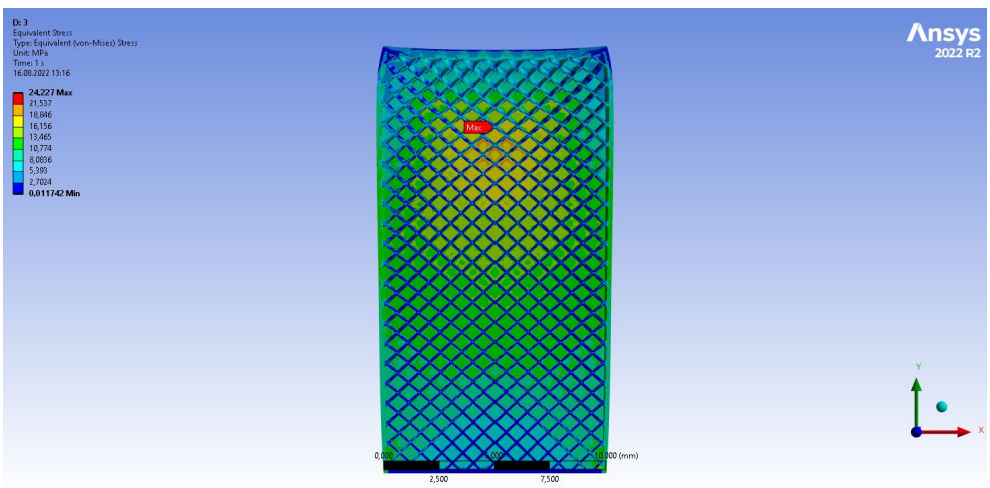

(b)

Figure 2: Max. Deformation (mm) and Von-Mises stress (MPa) of Configuration 3 (volume: 693.79 mm^3), infill ratio of 28%

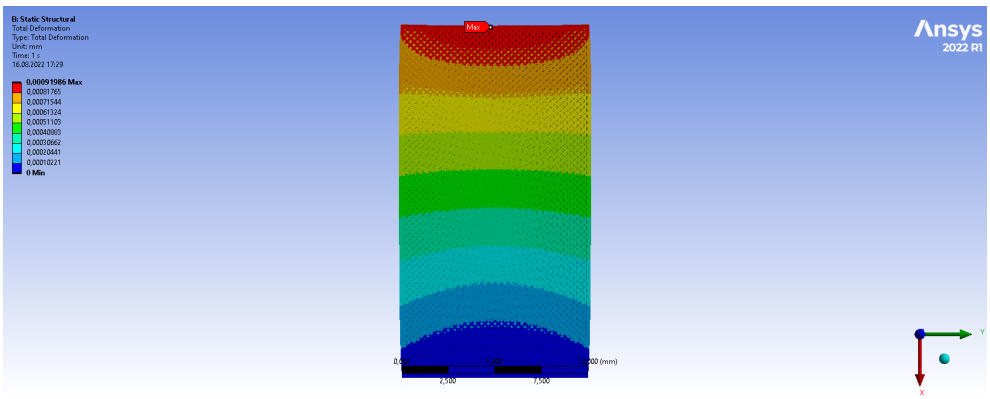

(a)

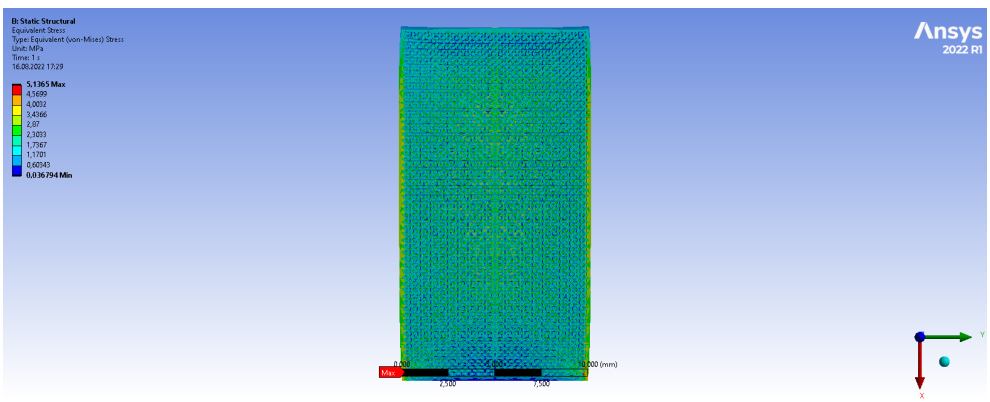

(b)

Figure 16: Max. Deformation (mm) and Von-Mises stress (MPa) of Configuration 4 (volume: 1348.4 mm^3), infill ratio of 64%

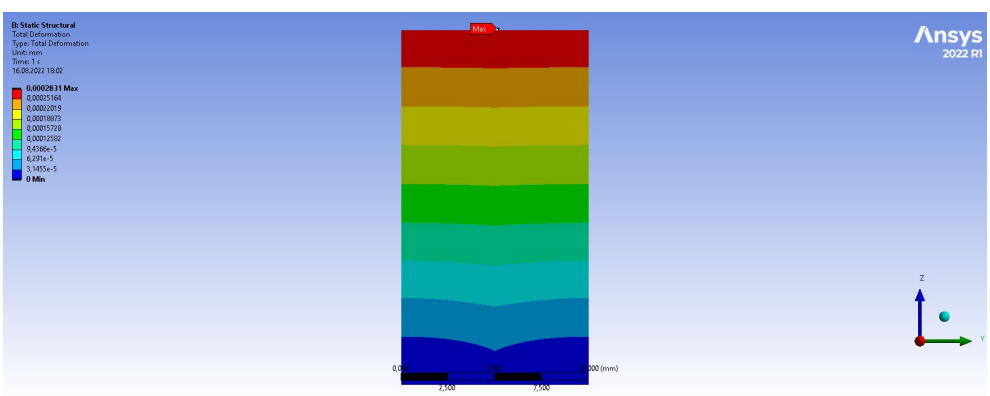

(a)

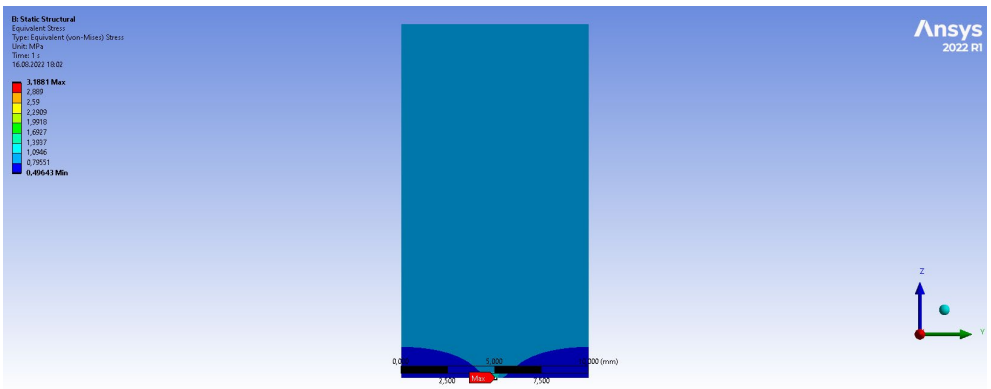

Figure 3: Max. Deformation (mm) and Von-Mises stress (MPa) of Configuration 5 (volume: 2000 mm^3), infill ratio of 100%

The change in maximum deformation in mm and maximum Von-Mises stress in MPa with respect to infill ratio are given in Figure 18 and Figure 19. It is shown that the maximum deformation and maximum Von-Mises stress values are reducing with the increasing infill ratio. It is interesting to note that changes in maximum values of deformation and Von-Mises stress values are non-linear with respect to infill ratio.

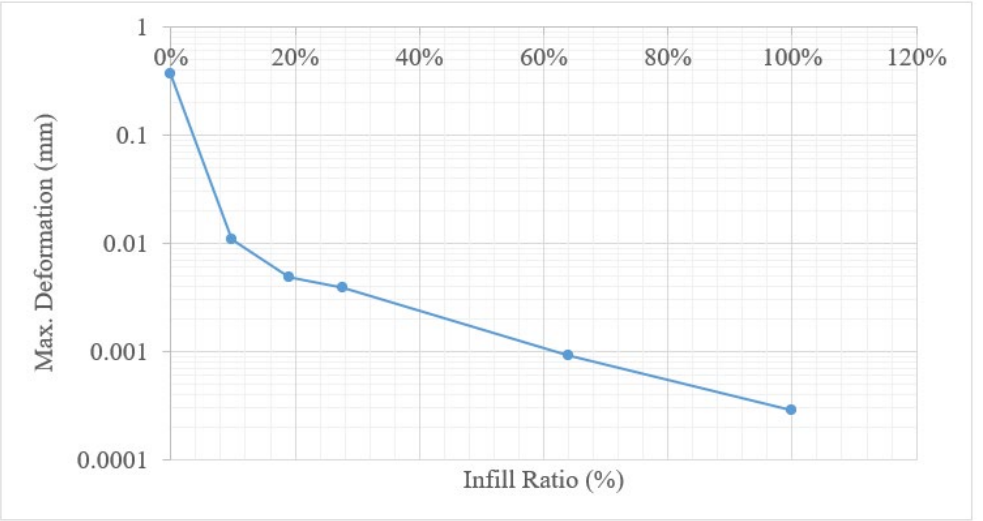

Figure 18: Maximum deformation (mm) values with respect to infill ratio.

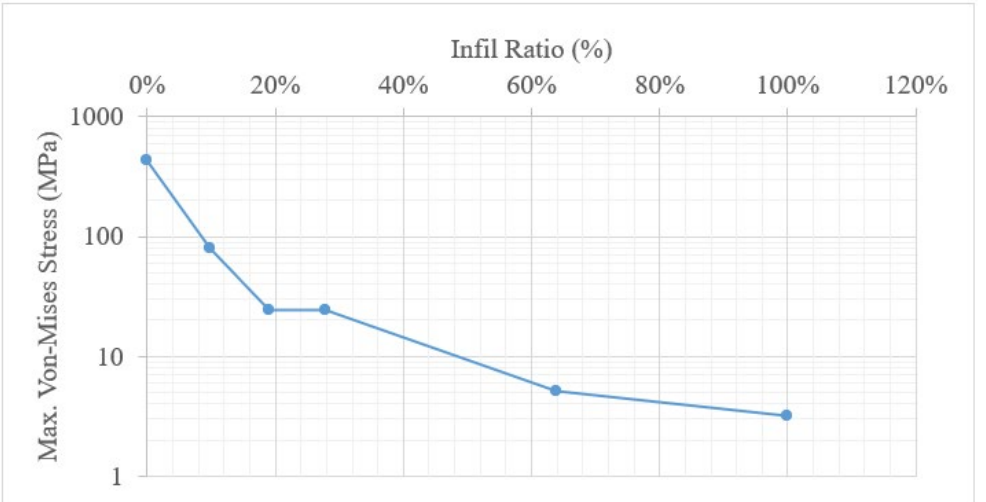

Figure 19: Maximum Von-Mises stress (MPa) with respect to infill ratio.

4. CONCLUSIONS

This study conducted the Finite Element Analysis of various infill densities of 0%, 10%, 19%, 28%, 64%, and 100% for deformation and Von-Mises stresses of a cuboid under compressional load. Mesh optimization was done by performing the mesh sensitivity analysis, and quarter symmetry was applied to reduce the computational load and time. Results revealed reduced Von-Mises stresses and deformation with increasing infill density percentage. These results are important for further infill optimization studies [22] to maximize the strength and minimize the weight of 3D printed parts. The presented study used a linear isotropic material property and set the basis for further studies with complex materials, i.e., non-linear and anisotropic material properties.

ACKNOWLEDGEMENT

The publication charges for this article have been funded by a grant from the publication fund of UiT The Arctic University of Norway

REFERENCES

[1] P. Miciński, J. Bryła, and A. Martowicz, “Multi-axis Fused Deposition Modeling using parallel manipulator integrated with a Cartesian 3D printer,” Int. J. Multiphys., vol. 15, no. 3, pp. 251–263, Jul. 2021.

[2] “Carbon Fiber Composite 3D Printer: Markforged Mark Two.” https://markforged.com/3d-printers/mark-two (accessed Sep. 27, 2022).

[3] H. Mei, Z. Ali, I. Ali, and L. Cheng, “Tailoring strength and modulus by 3D printing different continuous fibers and filled structures into composites,” Adv. Compos. Hybrid Mater., vol. 2, no. 2, pp. 312–319, Jun. 2019,

[4] Z. Andleeb, C. Strand, S. Malik, and G. Hussain, “Multiphysics Analysis of CFRP Charpy Tests by varying Temperatures,” Int. J. Multiphys., vol. 14, no. 2, pp. 143–160, 2020.

[5] Z. Andleeb et al., “Thermoelastic Investigation of Carbon-Fiber-Reinforced Composites Using a Drop-Weight Impact Test,” Appl. Sci., vol. 11, no. 1, p. 207, Dec. 2020.

[6] S. Ludvigsen, Z. Andleeb, H. Khawaja, M. Moatamedi, and B. Alzahabi, "Multiphysics Analysis of Contact Pressure Profile of Airless tires as compared to Conventional Tires," Int. J. Multiphys., vol. 14, no. 4, pp. 399–425, Nov. 2020.

[7] E. Stange, Z. Andleeb, H. Khawaja, and M. Moatamedi, "Multiphysics Study of Tensile Testing using Infrared thermography," Int. J. Multiphys., vol. 13, no. 2, pp. 191–202, Jun. 2019.

[8] H. Khawaja, "Application of a 2-D approximation technique for solving stress analyses problem in FEM," Int. J. Multiphys., vol. 9, no. 4, pp. 317–324, Dec. 2015.

[9] U. N. Mughal, H. A. Khawaja, and M. Moatamedi, "Finite element analysis of human femur bone," Int. J. Multiphys., vol. 9, no. 2, pp. 101–108, 2015.

[10] H. Eidesen, Z. Andleeb, H. Khawaja, and M. Moatamedi, "Multiphysics Analysis of Ice-Polyurethane Adhesion under Flexural Loading using FEM Analysis," Int. J. Multiphys., vol. 15, no. 4, pp. 437–452, Dec. 2021.

[11] E. Stange, Z. Andleeb, and H. A. Khawaja, "Qualitative visualization of the development of stresses through infrared thermography," Vestn. MGTU, vol. 22, no. 4, pp. 503–507, 2019.

[12] Z. Andleeb et al., "Multiphysics Study of Infrared Thermography (IRT) Applications," Int. J. Multiphys., vol. 14, no. 3, pp. 249–271, Sep. 2020.

[13] H. Norum, Z. Andleeb, H. Khawaja, and M. Moatamedi, "Determining Thermal Properties of Polyurethane by Solving the Heat Equation and IR Imaging," Int. J. Multiphys., vol. 16, no. 2, pp. 187–202, Jun. 2022.

[14] M. L. Dezaki, M. K. A. M. Ariffin, A. Serjouei, A. Zolfagharian, S. Hatami, and M. Bodaghi, "Influence of Infill Patterns Generated by CAD and FDM 3D Printer on Surface Roughness and Tensile Strength Properties," Appl. Sci. 2021, Vol. 11, Page 7272, vol. 11, no. 16, p. 7272, Aug. 2021.

[15] K. Wang, X. Xie, J. Wang, A. Zhao, Y. Peng, and Y. Rao, "Effects of infill characteristics and strain rate on the deformation and failure properties of additively manufactured polyamide-based composite structures," Results Phys., vol. 18, Sep. 2020.

[16] S. Ramakrishnan, C. John, and M. S. Anoop, "Numerical Analysis on Elastic Characteristics of 3D Printed Materials with Different Infill," pp. 677–693, 2023.

[17] "Choosing Infill Percentage For 3D Printed Parts, 3DPros." Accessed: Sep. 27, 2022. [Online]. Available: https://www.3d-pros.com/choosing-infill-for-3d-printed-parts

[18] B. S. Aadnøy and R. Looyeh, "Failure Criteria," Pet. Rock Mech., pp. 53–62, 2019.

[19] "Ansys, Engineering Simulation Software." https://www.ansys.com/ (accessed Dec. 12, 2021).

[20] D. Brunner, H. Khawaja, M. Moatamedi, and G. Boiger, "CFD modelling of pressure and shear rate in torsionally vibrating structures using ANSYS CFX and COMSOL Multiphysics," Int. J. Multiphys., vol. 12, no. 4, pp. 349–358, Dec. 2018.

[21] Z. Andleeb et al., "Strain Wave Analysis in Carbon-Fiber-Reinforced Composites subjected to Drop Weight Impact Test using ANSYS®," Int. J. Multiphys., vol. 15, no. 3, pp. 275–290, Jul. 2021.

[22] Z. Andleeb, S. Malik, G. Hussain, H. A. Khawaja, and M. Moatamedi, "Design optimization and dynamic testing of CFRP for helicopter loading hanger," Multiphysics Simulations Automot. Aerosp. Appl., pp. 187–209, Jan. 2021.